Available online at www.sciencedirect.com
ScienceDirect
European Journal of Pharmaceutics and Biopharmaceutics 69 (2008) 1121–1134
European Journal of Pharmaceutics and Biopharmaceutics
www.elsevier.com/locate/ejpb

Research paper

Development of microporous drug-releasing films cast from artificial nanosized latexes of poly(styrene-*co*-methyl methacrylate) or poly(styrene-*co*-ethyl methacrylate)

Daniel P. Otto [a,b,*], Hermanus C.M. Vosloo [c], Wilna Liebenberg [b], Melgardt M. de Villiers [a]

[a] *School of Pharmacy, University of Wisconsin – Madison, WI, USA*
[b] *Faculty of Health Sciences, North-West University, Potchefstroom, South Africa*
[c] *School of Chemistry, North-West University, Potchefstroom, South Africa*

Received 10 November 2007; accepted in revised form 1 February 2008
Available online 14 February 2008

Abstract

Two sets of copolymers comprising of styrene and either methyl or ethyl methacrylate as comonomer were conveniently synthesized by microemulsion copolymerization. The purified materials were characterized by GPC-MALLS and were shown to form artificial nanolatexes in THF. ATR-FTIR analysis revealed differences in copolymer composition and based on the copolymer properties, a selection of copolymers was chosen to cast drug-loaded, microporous films that exhibit microencapsulation of drug agglomerates. The contact angles of the copolymers suggested potential applications in medical devices to prevent the formation of bacterial biofilms that commonly result in infections. Additionally, the different copolymeric films showed two phases of drug release characterized by a rapid initial drug release followed by a zero-order phase. Depending on the application, one could select the copolymer films that best suited the application i.e. for short-term drug release applications such as urinary catheters or long-term applications such as artificial implants.

Keywords: Methacrylate copolymer; Microencapsulation; Film; Rifampin; Controlled release

1. Introduction

Several studies have reported the introduction of infections in patients which received polymer-based medical devices, i.e. orthopedic surgical implants [1], urinary catheters [2], cardiovascular stents [3] and ventilator-associated pneumonia with use of endotracheal tubes [4]. The procedures associated with the use of these devices are invasive and compromise natural barriers of the body that protect it from infection [5].

In the event of bacterial accumulation, a so-called biofilm is created on a surface, i.e. a polymer film or coating. This biofilm is often a very resistant and physically strong structure comprising several stacked layers of microorganisms [6]. Once the biofilm has been established the onset of an infection could be observed. Therefore, the development of strategies to curb infections associated with the use of polymeric devices is warranted if the devices should actually benefit, not compromise, the health of patients [7,8]

Circumvention of biofilm formation could entail a number of approaches. Some techniques modify the surface chemistry of the polymer film to hinder bacterial attachment by methods such as thiocyanation since thiol groups could be microbiocidal [9]. Other methods employ loading the polymer device with antimicrobial agents, i.e. rifampin, fusidic acid and mupirocin combinations [10], rifampin and minocycline [11], gentamicin [12,13], vancomycin [14] and ciprofloxacin [15] that release low quantities of the drugs over prolonged periods that effectively eradicate the biofilm.

Several tests could be conducted to establish the surface properties and the contact angle of the polymer film could

* Corresponding author. School of Pharmacy, University of Wisconsin – Madison, 777 Highland Avenue, Madison, WI 53705, USA. Tel.: +1 608 262 9351.
E-mail address: dotto@wisc.edu (D.P. Otto).

0939-6411/$ - see front matter © 2008 Elsevier B.V. All rights reserved.
doi:10.1016/j.ejpb.2008.02.004

serve as a first, although not absolute, indicator of the potential adhesion properties of bacteria onto film surfaces. Bacteria usually adhere to polymer substrates of similar hydrophobicity or hydrophobicity [16,17].

A convenient way to produce a polymer film is by solvent casting of a pseudolatex or artificial latex [18] produced from a characterized material. The production of a film from a pseudolatex is advantageous since unwanted monomer and other materials or remnants from polymerization reactions could be removed from the material before it is used [19].

At the molecular level, it is very difficult to truly blend polymer materials and one of the classic examples of phase separation occurs in blends of poly(methyl methacrylate) (PMMA) and poly(styrene) (PS) [20,21]. Despite the incompatibility of PS and PMMA, it might be advantageous to incorporate different polymers comprised of methacrylate and styrene units to modify an application. Both PS and PMMA have found applications in prostheses fixation and drug delivery from these prostheses and it would be of value to investigate the effect of a copolymer composed of both monomers of these polymers.

A method to produce a true blend of different monomers (and therefore avoid phase separation) is by copolymerization of the desired monomers. It was shown that the phase separation observed for the blends of poly(styrene) and poly(methyl methacrylate) was not observed for a copolymer of styrene and methyl methacrylate [22]. Furthermore, copolymers consisting of monomers corresponding to those found in immiscible homopolymers could act as compatibilizers to augment miscibility [23]. Microemulsion copolymerization lends itself to the production of nanoscale random copolymer latexes which could be purified to produce a final copolymeric material comprising the desired chemical composition [24].

Several random copolymers are available that incorporate methacrylic monomers. Typical examples of non-ionic random methacrylic copolymers in the pharmaceutical industry are marketed as Eudragit® NE and MN that have been applied in various film coatings for numerous purposes including taste-masking and controlled release of drugs [25].

Some applications could be found for poly(styrene-*co*-methyl methacrylate) (P(St-*co*-MMA)) as bone cement i.e. Endurance® cement [26]. However, no pharmaceutical application could be found for poly(styrene-*co*-ethyl methacrylate) (P(St-*co*-EMA)) copolymers. Subsequently, P(St-*co*-EMA) and P(St-*co*-MMA) copolymers were synthesized, characterized and evaluated for potential pharmaceutical applications.

2. Experimental section

2.1. Materials

Rifampin (RIF) was purchased from Youhan Corp. (Seoul, Korea). The homopolymers used in this study PMMA, poly(ethyl methacrylate) (PEMA) and PS (Scientific Polymer Products, Inc., Ontario, NY). Copolymers comprising styrene and either methyl or ethyl methacrylate were synthesized by microemulsion copolymerization. Tetrahydrofuran (THF) (Fisher Scientific, Pittsburgh, PA) was used as solvent for all the polymers and RIF.

2.2. Copolymerization procedure

The microemulsion copolymerization was conducted according to a 3-level-4-factor fractional factorial design applying some formulation guidelines provided in the literature [27]. Briefly the reactions employed double deionized water (qs 100% wt.) (Milli-Q®, Microsep, Sandton, South Africa) as dispersion medium with ultrapure sodium dodecyl sulfate (SDS) (Sigma–Aldrich, Kempton Park, South Africa) as surfactant (2–8% wt.). The cosurfactant, 1-butanol (BuOH) (Merck, Modderfontein, South Africa) was incorporated in all reaction mixtures at levels between 1–5% wt. Potassium persulfate (KPS) (Sigma–Aldrich, Kempton Park, South Africa) was used as the reaction initiator at 0.5% wt. for all reactions. A mixture of 60–80% of styrene (St) (Merck, Modderfontein, South Africa) and 20–40% either methyl methacrylate (MMA) or ethyl methacrylate (EMA) (donated by Degussa, Düsseldorf, Germany) was added to the reaction medium. These monomer mixtures constituted 6% wt. of the total reaction mixture and were copolymerized for 2 h. The reactions were performed at a specified temperature between 60 and 80 °C. All reactions were performed with magnetic stirring at 500 r.p.m. under continuous N_2 purge. An excess of hydroquinone (Sigma–Aldrich, Kempton Park, South Africa) was added to quench the reaction after 2 h.

The copolymer latexes were a translucent blue color, indicating the existence of very fine colloidal particles. The latex was precipitated with copious quantities of methanol (MeOH) (Merck, Modderfontein, South Africa). The mixtures were vortex-shaken (Vortex Genie 2®, Daigger®, A. Daigger and Company, Vernon Hill, IL) and centrifuged in 50 cm^3 tubes at 3500 r.p.m for 10 min. The sediments were subsequently redispersed and washed with MeOH followed by centrifugation until no redispersion could be effected by addition of MeOH.

Susequently, the copolymers were dried in a fume hood until only brittle material remained. These white products were finely pulverized and then dried for an additional 24 h under a vacuum of 13 mbar. The powders were then sealed in opaque, airtight containers until further use.

2.3. Copolymer characterization

2.3.1. GPC-MALLS

GPC-MALLS was utilized to characterize the absolute molecular weight and particle size of the polymer samples. A DAWN® DSP laser photometer (Wyatt Corporation, Santa Barbara, CA) and a refractive index detector (Agilent® 1100 series) were used as detectors. Briefly, 100 μL of 3 mg/mL polymer samples dissolved in THF were injected into the GPC columns (PLGel® mixed bed type

C™, 7.6 × 300 mm, exclusion range 300–2 000 000 g mol^{-1}, particle size of 5 μm and a Phenogel™ Phenomenex®, 7.8 × 300 mm, exclusion range >5000 g mol^{-1}, particle size of 5 μm, Separations Scientific CC, Honeydew, South Africa) with THF as a mobile phase. The weighted molecular weight and radii of gyration averages (Eqs. (1 and 2)) as well as conformation of the copolymer chains were calculated from the scattering data (Eq. (3)) (ASTRA™ 4.73, Wyatt Corp.) according to the Zimm formalism employing all MALLS scattering angles between 17° and 155° [28]:

$$\frac{R_\Theta}{Kc} = MP(\Theta) - 2A_2cM^2P^2(\Theta) + \cdots \quad (1)$$

where M is the molecular weight of a slice of the sample chromatogram, R_Θ is the excess Rayleigh ratio at the scattering angle Θ. Additionally, the wavelength and scattering angle-dependent particle scattering factor is represented by $P(\Theta)$. Furthermore, the concentration of the particles is denoted as c (determined with the refractive index detector) and A_2 is the second virial coefficient which becomes negligible at low concentrations as employed here). The constant K was derived by employing Eq. (2):

$$K = \frac{4\pi^2 n_0^2}{\lambda_0^4 N_A}\left(\frac{dn}{dc}\right)^2 \quad (2)$$

where the refractive index of the solvent in vacuum is n_0 at the incident wavelength of the vertically polarized laser radiation, λ_0, the Avogadro number is N_A and the specific refractive increment of the polymer is dn/dc.

Evaluation of the linear segment of the data if plotted as a double-logarithmic plot and fitted to a power law regression according to Eq. (3):

$$\langle S^2\rangle^{1/2} \propto M_w^q \quad (3)$$

where the z-average root mean square $<s^2>^{1/2}$ radius was related to the weight average molecular weight M_w.

2.3.2. ATR-FTIR

The composition of the copolymer particles was determined with attenuated total reflectance Fourier transform infrared spectroscopy (ATR-FTIR). The ATR-FTIR (Bruker, Ettlingen, Germany) comprised a ZnSe crystal and a microsample accessory. Sufficient quantities of the samples were transferred to the crystal sample accessory and clamped onto the crystal. 32 spectra were collected at a spectral resolution of 4 cm^{-1} for each sample. Wave numbers could be assigned for quantitative analysis, i.e. the out-of-plane bending of the phenyl ring in styrene units at ~699 cm^{-1} and the saturated alkyl ester carbonyl of the methacrylates at ~1729 cm^{-1} [29]. Monodiperse, low weight standards of PMMA and PS (Fluka, St. Louis, MO) were prepared to contain various mole fractions of St and either MMA and EMA.

2.3.3. Film casting

Following the synthesis of the copolymers, analysis of the polymers by GPC-MALLS and ATR-FTIR revealed suitable candidates for application in film casting. Pseudolatexes of the homopolymers and copolymers were prepared in THF (5% w/v) by sonication, allowing a 12 h swelling period. RIF was dissolved in THF (5% w/v) before film casting. The requisite quantities of the synthesized copolymer or homopolymer and drug solution were mixed to produce mixtures of 20% drug/80% polymer.

These solutions were cast onto previously cleansed, weighed glass surfaces and left to slowly dry under ambient conditions at 23 °C for 12 h followed by additional drying in a vacuum oven at 40 °C for 12 h (to obtain constant weights). The complete film cast with glass surface was weighed to determine the weight of the film. Strips measuring 6 × 2.5 cm were cut and weighed. The theoretical amount of drug in the strip was calculated. Film strips were stored in a desiccator preceding additional evaluations of the films.

2.4. Film characterization

2.4.1. Scanning electron microscopy

Scanning electron microscopy (SEM) studies were performed on film samples taken before and after release studies. These samples were affixed on carbon-taped stubs and thinly coated with Au/Pd in an Argon-filled bell jar under vacuum of ~130 Torr. A Hitachi S570 was used to photograph the samples employing Gatan DigitalMicrograph™ imaging software (Gatan, Inc., Warrendale, PA). All micrographs were recorded with a crystal emission of 10 keV. Additional SEM micrograph analysis was conducted with automated image analysis routines utilizing ImageJ 1.38× imaging analysis software [30].

2.4.2. Contact angle

Contact angle measurements were made by carefully depositing a drop of 10 μL of deionized water or release medium on various spin-coated films of the (co)polymers or (co)polymer/drug solutions. The droplet was photographed via a remote-controlled digital camera (Canon USA, Inc., Lake Success, NY) that was interfaced with a computer. The obtained images were analyzed with ImageJ 1.38× to measure the contact angle [31,32].

2.4.3. Release studies

Drug release from the films was evaluated in triplicate according to the USP apparatus II basket rotation method utilizing a VanKel VK 7000 dissolution tester (VanKel Technology Group, Edison, NJ) adjusting the rotational speed to 50 r.p.m. phosphate buffer (500 cm^3) (USP XXIX 2006 [33]), pH 7.40, served as the release medium and was maintained at 37 ± 0.5 °C. Samples (5 cm^3) were collected at predetermined intervals over a 24 h period through 0.45 μm MCE membrane syringe filters (Fisher Scientific, Pittsburgh, PA) and release vessels were immediately replenished with 5 cm^3 fresh buffer. Samples were analyzed by UV spectrophotometry at a wavelength of 333 nm [34,35] with a Beckman DU® 640 UV/Vis spectrophotometer

(Fullerton, CA). Linear calibration curves could be constructed in the range 0.5–40 μg/mL RIF ($r^2 > 0.9999$) using the release medium as solvent and blank. Different release kinetics models were used to investigate the release mechanism of the drug from the films:

The Peppas-model [36,37]:

$$\frac{M_t}{M_\infty} = Kt^n \tag{4}$$

where M_t is the amount of drug released at time t, and M_∞ is the amount of drug that is released after infinite time-lapse, therefore approaches the maximum potential release. K is a constant and n is the exponent characterizing the release process. If typical Fickian diffusion was observed, n would assume values of 0.5, 0.45 and 0.43 for thin films, cylinders and spheres, respectively. This equation should be used carefully as with all other power law descriptions to model release up to the fraction $M_t/M_\infty < 0.6$

Higuchi-model ([38, 39]:

$$M_t = A[D(2C_0 - C_s)C_s]^{1/2} \tag{5}$$

where M_t is the amount of drug release until time t, A defines the release area, D is the drug diffusion coefficient, C_0 is the initial concentration of the drug in the delivery system and C_s denotes the solubility of the drug.

A zero-order release kinetics model could also be applied in the secondary release phase [40,41]:

$$C_t = C_0 - k_0 t \tag{6}$$

where C_t is the concentration of the drug that is released at time t, C_0 is the initial concentration of the drug incorporated in the delivery device, k_0 is the zero-order release constant that describes the constant release rate for any time point in a zero-order release phase.

3. Results and discussion

3.1. Copolymers

3.1.1. Copolymer molecular weight, radius of gyration and conformation

The properties of the synthesized copolymers are listed in Table 1. Two replicates of 27 copolymers were synthesized for each monomer pair and analyzed to determine their molecular weight, polydispersity, radius of gyration, conformation and chemical composition. Statistical analysis of the factorial design revealed that the cosurfactant dominated the molecular weight properties as well as determined the size of the polymer chains.

The effect of the cosurfactant on M_w (Fig. 1) was clearly not similar for both series of copolymers. A linear increase in polymer weight of P(St-*co*-MMA) was seen with weight ranging from 250 to 700 kg mol^{-1} (considering the standard deviation error bars) as the concentration of BuOH increased. The P(St-*co*-EMA) series demonstrated weights ranging 190–550 kg mol^{-1} (considering the standard deviation error bars). At the highest concentration of BuOH, P(St-*co*-EMA) copolymers had the lowest weight and this was the only point where significant differences in weight was seen, although the P(St-*co*-EMA) polymers were comparatively lighter than the P(St-*co*-MMA) produced under the same conditions.

The effect of BuOH on $<s^2>^{1/2}$ (Fig. 2) paralleled the effect on M_w as can be seen from the linear increase in $<s^2>^{1/2}$ for P(St-*co*-MMA) versus the parabolic continuance for P(St-*co*-EMA). All the copolymer particles illustrated sub 50 nm values for $<s_2>^{1/2}$ with P(St-*co*-EMA) ranging between 20 and 26 nm and P(St-*co*-MMA) between 25 and 37 nm.

Based on the HLB value of 7.0 for BuOH [42] one could envision that micelles clustered together during the polymerization since BuOH would reside in the surfactant alkyl

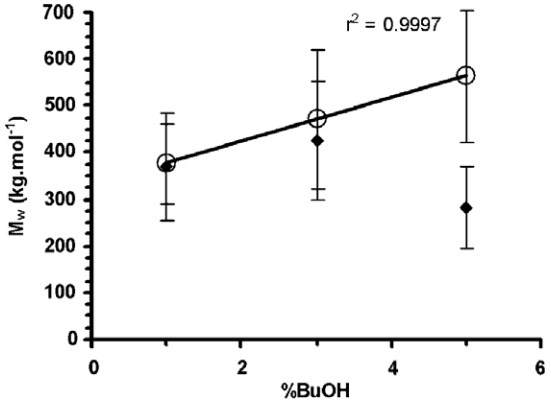

Fig. 1. The effect of the cosurfactant on M_w of (○) P(St-*co*-MMA) and (♦) P(St-*co*-EMA) copolymers.

Table 1
Properties of the copolymers synthesized by microemulsion copolymerization

Polymer	M_w (kg mol^{-1})	M_w/M_n	$<s^2>^{1/2}$ (nm)	q	%MMA	%St
P(St-*co*-MMA)						
1	474.2	1.8	32	0.492	19	81
2	309.1	1.8	23	0.502	37	63
3	183.1	1.8	18	0.459	52	48
P(St-*co*-EMA)					%EMA	
1	244.0	2.0	22	0.500	14	86
2	217.5	1.8	18	0.458	24	76
3	314.6	1.8	18	0.527	34	66

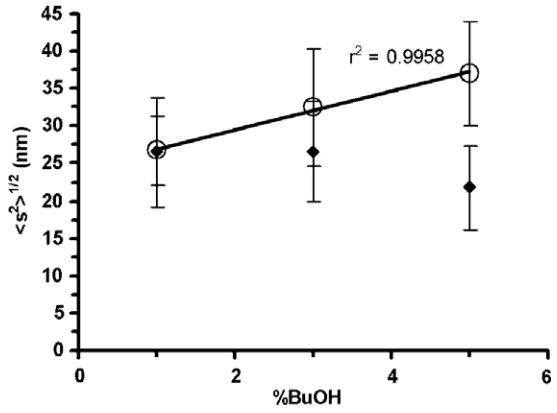

Fig. 2. The effect of the cosurfactant on $\langle s^2\rangle^{1/2}$ of (○) P(St-*co*-MMA) and (♦) P(St-*co*-EMA) copolymers.

tail in the interface of the micellar reactors. The local concentration of the monomers would therefore increase as BuOH concentration increased and P(St-*co*-MMA) molecular weights increased. At the highest concentration of BuOH, the partitioning of EMA (more hydrophilic than styrene) to the interface is limited. Subsequently, a decrease in monomer oligomer radicals formed in the interface, reducing radical entry into the monomer swollen micelles (reaction locus) that could nucleate the micelles [43].

The conformational analysis (Fig. 3) was performed to determine the suitability of the solvent, THF, to disperse the polymer chains. The conformation was determined with consideration of the limitation of MALLS detection of small particles below ~20 nm [44–46]. The polymers predominantly illustrated conformation values of $q \approx 0.4$–0.5. The samples indicating a q value of ~0.5 were selected, since these illustrated the ideal θ conformation.

The θ condition for a polymer chain dispersed in a solvent is found at a specific temperature (in this case ambient temperature) and could be compared to the state at which a sample would start to melt [47]. This indicated that both the intra- and intermolecular attractive forces were in equilibrium and that polymer chains could interpenetrate each other freely with no resultant interaction [48].

Therefore optimal copolymer dispersion would occur in THF if copolymers were chosen that illustrated conformations close to the θ condition, facilitating the mixture with a drug solution in THF. Not surprisingly, these copolymers were found in the lower weight range of both sets.

Studies found that melting of RIF resulted in decomposition of the drug [34,35,49]. Furthermore, the copolymers melt at temperatures higher than the melting point of RIF, precluding the melting method for producing films. Subsequently THF solutions of the selected copolymers and RIF could be utilized for solvent casting of films. Additionally, THF is a volatile, pharmaceutically acceptable class III solvent [50].

3.1.2. Copolymer composition

The statistical analysis revealed that copolymer composition was determined solely by the monomer feed composition (Fig. 4, Table 1). It was argued that the clustering of micelles, induced by BuOH would ultimately determine the number of radicals that could nucleate the micelles and therefore determine the molecular weight of the copolymer particle. However, MMA is slightly more hydrophilic than EMA and therefore MMA partitioned to a higher extent to the interface where primary radicals were formed that could nucleate the micelles. This also reflected in the composition, since lower fractions of St were found in the corresponding copolymer. Subsequently higher fractions of St were found in the P(St-*co*-EMA), indicating that both monomers resided to a larger extent in the micelle compared to the uneven partitioning of MMA systems.

3.2. Films

3.2.1. Morphology

The cavities of the honeycomb structures of P(St-*co*-MMA) films had Feret-diameters ranging from 12 to 17 μm, circumferences ranging 40–73 μm, and projected

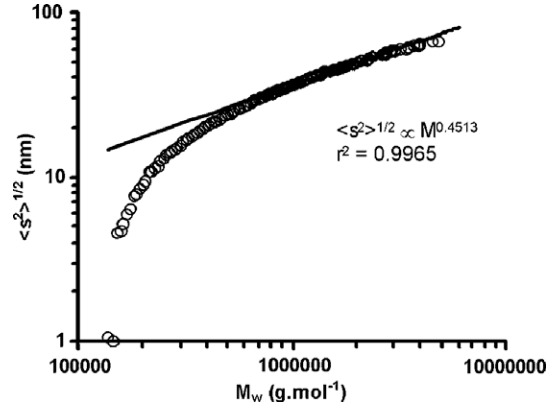

Fig. 3. Conformation plot of P(St-*co*-MMA) comprising of 37% MMA and 86% St. The power law regression was performed by negating the uncertainties for particles under 20 nm.

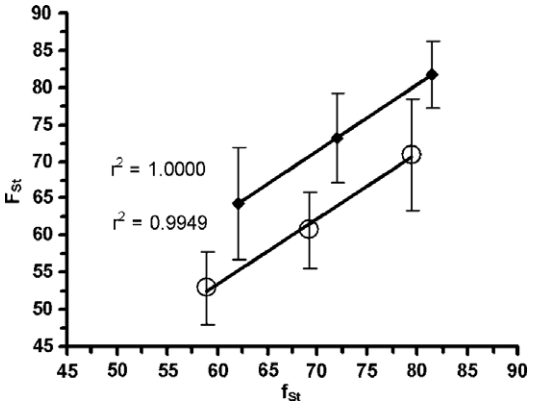

Fig. 4. The effect of the feed fraction of St on the polymer fraction of St for (○) P(St-*co*-MMA) and (♦) P(St-*co*-EMA) copolymers.

areas of 89–98 μm^2 resulting from an increase in MMA content from 18% to 52%. P(St-*co*-EMA) films had cavity Feret diameters of 4.6–5.9 μm, perimeters of 14–19 μm with projected areas of 15–20 μm^2 as EMA content increased from 14% to 34%. Fig. 5A and B shows that the surface cavities of P(St-*co*-MMA) was approximately double the size of those found for P(St-*co*-EMA). In addition all these cavities exhibit circularities of 0.9–1.0, indicating that an oblong to circular type of shape could describe the cavities. The P(St-*co*-EMA) films therefore seemed more porous and the P(St-*co*-MMA) films more dense.

The honeycomb structure of the films (Fig. 6) evolved due to a complex set of events. The solubility parameters (δ in MPa$^{1/2}$) based on the Hansen and Hildebrandt methods were found in literature for THF ($\delta = 18.6$–19.47) [51,52], RIF ($\delta = 20.76$) [53], PS ($\delta = 18.19$) [51], PMMA ($\delta = 19.65$) [51], PEMA ($\delta = 20.46$) [52] and the corresponding copolymers ($\delta = 18.85$) [51]. These values indicated that these materials would all be miscible in a THF solution since the values of $\Delta\delta$ was small – a prerequisite for miscibility [54].

The free energy of the mixing theory [47] was applied to explain the morphology of the drug-loaded films:

$$\Delta G_{\mathrm{m}} = \Delta H_{\mathrm{m}} - T\Delta S_{\mathrm{m}} \tag{7}$$

where ΔG_{m} is the free energy of mixing and should be negative to favor mixing, ΔH_{m} is the exothermic mixing enthalpy (therefore if spontaneous, it should be negative), T is the Kelvin temperature and ΔS_{m} is the mixing entropy (which should be positive to show and increase in the disorder, therefore mixing in the system).

According to the Flory–Huggins theory [47], the heat of mixing is determined by the volume fraction of each component that should be mixed as well as the solubility parameter of each component. Furthermore, the interaction energy between the polymer and solvent is described by the interaction parameter. Eq. (8) was derived [47] to describe the free energy of mixing in a polymer–solvent system:

$$\Delta G_m = RT(n_1 \ln \phi_1 + n_2 \ln \phi_2 + \chi\, n_1\phi_2) \tag{8}$$

where ΔG_{m} is the free energy of mixing, R and T are the universal gas constant and absolute temperature respectively, n_1 and n_2 are the molar quantities of the solute and solvent, respectively, ϕ_1 and ϕ_2 and χ is the interaction parameter of the solute and the solvent.

In Eq. (8) the first two terms represent the enthalpy of mixing and the third term the entropy of mixing. For the following argument, RIF should be seen as a small oligomer that is monodispersed (RIF has a molecular weight of 822.94 g mol^{-1}) and in combination with the copolymer, formed the polydisperse component 1 (Eq. (8)). Additionally, the molecular weight of this oligomer is much lower than any of the copolymer fractions (the M_{w} of the copolymers was $\sim 10^5$ g mol^{-1}, Fig. 3), therefore not overlapping with any copolymer weight fraction. Finally, due to the weight polydispersity of component 1, χ should be summed as an index of the different weight fractions [47].

When casting the film, the solvent starts to evaporate and subsequently the interaction between the solute component and solvent becomes weaker and the interactions between the solute components increase (θ condition dissipates). Additionally, the volume fraction of the solvent decreases upon evaporation. Ultimately, ΔG_{m} becomes less negative, mixing becomes improbable and therefore phase separation occurs [55].

Phase separation also occurs as a series of steps with the higher weight copolymer fractions showing the highest propensity to precipitate, followed by lower weight fractions. During this process of precipitation, the polymer latex extrudes some of the THF, producing two liquid phases. One phase is rich in the polymer fraction that is about to precipitate, the other is richer in solvent and species less prone to precipitate, i.e. the oligomer [55]. This coacervation phase finally results in numerous liquid-filled pockets in the film. Since the oligomer was still encapsulated in these pockets, the oligomer finally precipitated in these pockets once the solvent evaporated. Consequently, a film

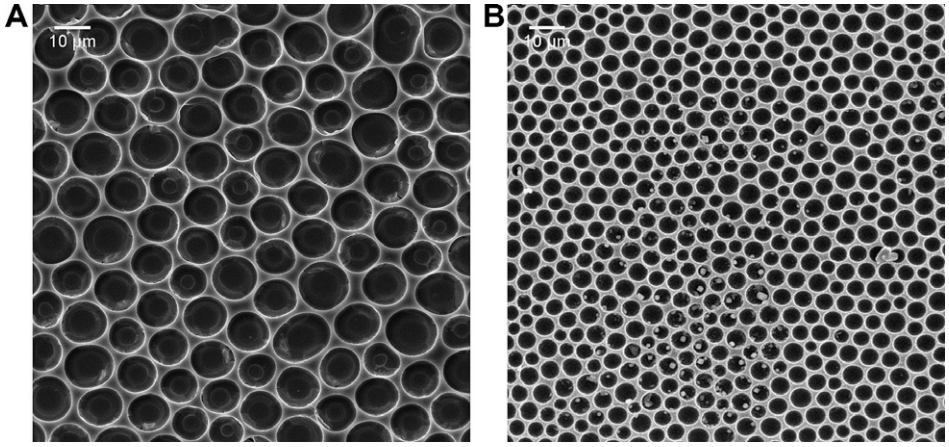

Fig. 5. Top surface cavities of blank films of (A) P(St-*co*-MMA) (52% MMA) and (B) P(St-*co*-EMA) (14% EMA).

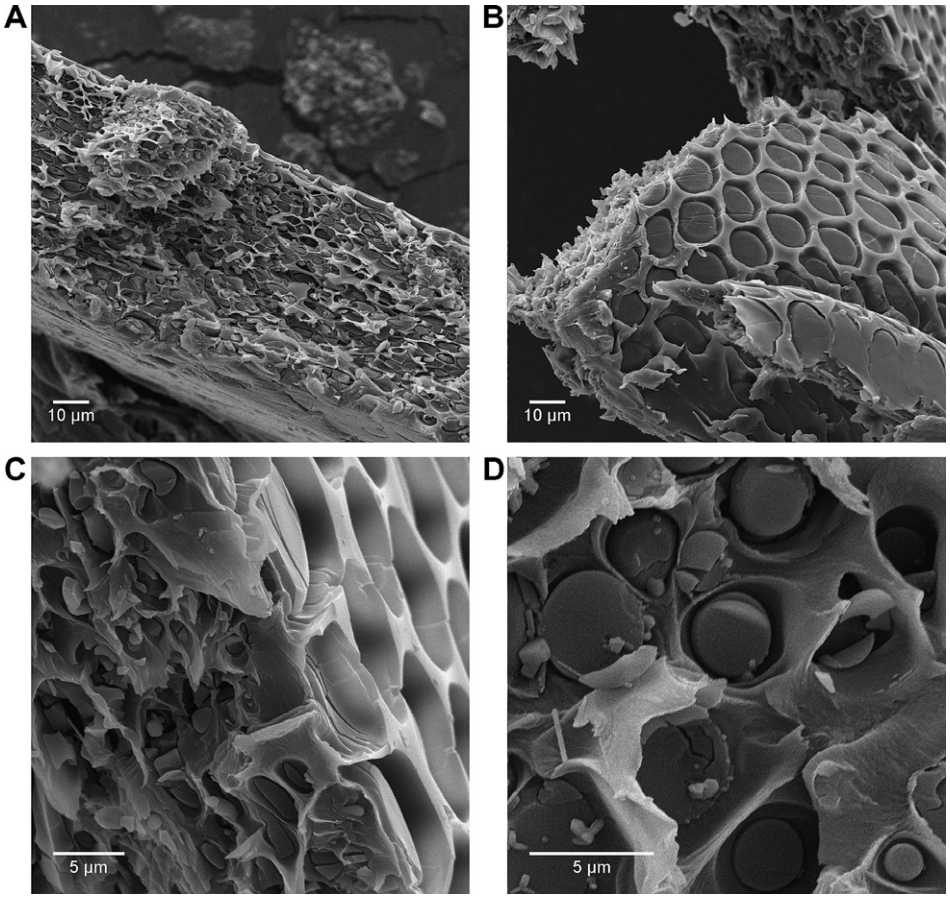

Fig. 6. (A) Cross section of RIF-loaded P(St-*co*-MMA) films (37% MMA) (A) honeycomb structure before release, (B) tilted view of the film after release and (C) magnified cross sectional view of the film after release. (D) Cross-section of P(St-*co*-EMA) (14% EMA) showing that RIF was still present in the micropockets after a release period of 24 h.

with polymer-encapsulated drug micropockets assembled into a honeycomb structure.

4. ATR-FTIR characterization

ATR-FTIR spectra were recorded for the copolymer films before and after loading with RIF (Fig. 7). The characteristic peaks of rifampin were identified as the symmetric (C—O—C acetyl) ~1020 cm^{-1} vibration, the amide II vibration at ~1534 cm^{-1}, the (C=C) vibration at ~1565 cm^{-1}, the amide I vibration at 1650 and 971 cm^{-1} [34,35,56]. The characteristic phenyl ring out-of-plane bending for styrene was observed at 699 cm^{-1} and the characteristic saturated alkyl ester carbonyl stretch was observed at 1729 cm^{-1}. Rifampin showed its characteristic carbonyl stretch in the same spectral region as the methacrylate ester and therefore the spectra were significantly overlapped in this region, although these peaks did not shift. Note that Form II of RIF shows 2 peaks in the carbonyl region at 1712 and 1730 cm^{-1} whereas the amorphous form showed only 1 peak at 1725 cm^{-1}.

Form II is the typically found crystalline form of the drug found in several commercial samples. Earlier studies, showed that amorphous form (as determined by X-ray diffraction) showed a single peak in the carbonyl ester region. The crystalline form (form II) (as previously investigated by X-ray diffraction) showed two pronounced peaks in the carbonyl region [35,36].

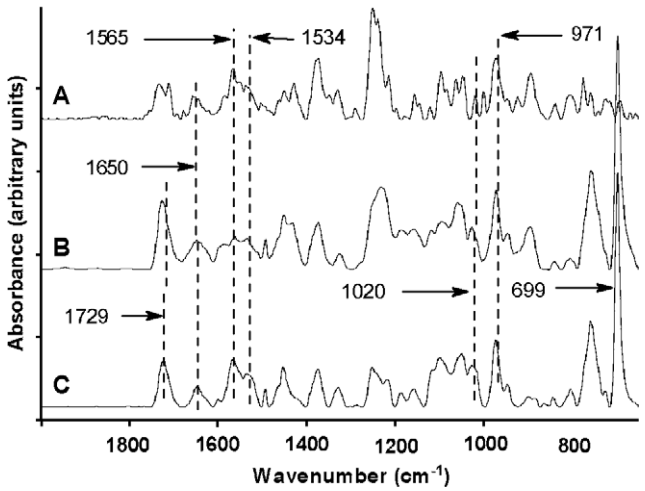

Fig. 7. Expanded ATR-FTIR spectra of (A) RIF Form II and RIF-loaded copolymer films of (B) P(St-*co*-MMA) (19% MMA) and (C) P(St-*co*-EMA) (14% EMA).

This suggested that no interactions could be detected between RIF and the copolymers. Additionally, the SEM micrographs in Fig. 6, illustrated that drug molecules were present in the micropockets as seen from the agglomerate spheres. This confirmed findings that RIF did not interact with methacrylate-based non-ionic Eudragit® copolymers [57,58].

4.1. Contact angles

The contact angles of all the homopolymers were fairly high at around 80°, indicating a hydrophobic character. The contact angle of rifampin that was spin-coated from a THF solution also indicated a poor wetting ability from an angle of 70°. From these findings one would expect that the copolymers should possess the same hydrophobicity. One would also expect that the inclusion of RIF would not affect the contact angle significantly.

However, Fig. 8 depicted that the contact angles that were obtained contradicted these expectations. Of note was that the inclusion of RIF resulted in a decrease in the contact angle of the film relative to the blank polymer film. This could indicate a potential application of the drug solely for decreasing the contact angle, thus minimizing the accumulation of bacteria. The decrease in contact angle with the incorporation of RIF was observed for both the P(St-*co*-EMA) and P(St-*co*-MMA) copolymer films. Additionally, the contact angles for the blank P(St-*co*-EMA) films showed a linear decrease as the content of EMA was increased producing angles from 80° to 55°. However, blank P(St-*co*-MMA) films produced consistent contact angles despite the variation in MMA content.

The contact angle of the liquid on a particular surface could be indicative of the adhesion potential between the two phases. These surfaces could include a polymer surface as well as a bacterial culture surface. As a general rule, if the contact angles of a bacterial species and polymer substrate surface do not match as evaluated by the same liquid (i.e. buffer or water), then the adhesion of a bacterial species would be penalized. This would be an advantageous property of the polymer film to prevent the initial adhesion of the bacteria to the polymer surface and subsequently stunt the development of a biofilm which ultimately results in infection.

Furthermore, if the contact angle of the surface decreases, it implies that the wetting of the surface is better and that solvent might wet the drug particles on the surface to higher extent, with a higher rate of release of surface-located drug molecules. This initial high release could also prevent the initial adhesion of bacteria due to an antiseptic effect (even below the therapeutic concentration of the drug).

Seen from the perspective of the contact angles, the application of the copolymers would pose an advantage compared to homopolymer films with regard to limiting bacterial biofilm formation of certain bacterial strains. It is known that hydrophobic bacteria, i.e. *Pseudomonas aeruginosa* would preferentially adhere to a hydrophobic substrate compared to hydrophilic *Staphylococcus liquefaciens* that prefer hydrophilic surfaces [17]. The copolymer films produced in this study could find application in the prevention of adhesion of species such as *P. aeruginosa*.

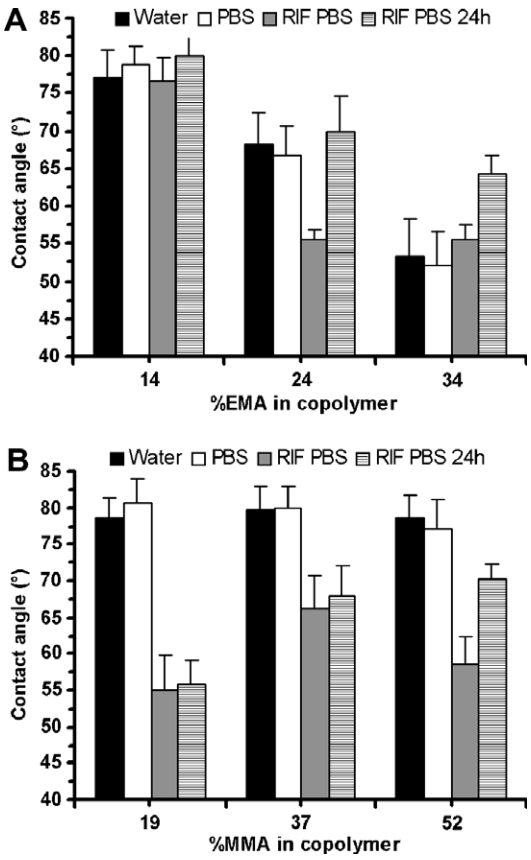

Fig. 8. Contact angles of (A) EMA and (B) MMA copolymers that were spin-coated onto glass surfaces. RIF indicates the films loaded with rifampin and the films after 24 h release is indicated as RIF PBS 24 h. PBS is phosphate buffer solution at pH 7.4 (dissolution medium). Error bars indicate standard deviations.

5. Release studies

5.1. Homopolymer films

The films demonstrated that they possessed favorable properties regarding contact angles and the possible application to limit biofilm formation. The question, however arose whether the contact angle would affect the drug release pattern as well.

An attempt was made to load PS, PMMA and PEMA with 20% drug followed by monitoring the release of RIF over a 24 h period (Fig. 9). The release studies revealed that the loading of the poly(methacrylate)s was more successful than that seen for the PS film as observed from the initial release of drug from the films.

The PS films released approximately 20% of the drug in the first hour of the 24 h period followed by a seemingly negative release or in fact no release in the remainder of the study. It was therefore predicted that fairly quick release would be seen if high styrene content was found in the copolymers. The PEMA and PMMA films released approximately 3% and 6%, respectively, in the first hour followed by no obvious release or more erratic release as seen from the fluctuation in release values for the remainder of the 24 h period (Fig. 9). No time-correlated release patterns could be observed for these homopolymer films since zero-order and Higuchi kinetics demonstrated poor fits of the release curves with $r^2 < 0.5$.

It would however seem that the incorporation of a methacrylate monomer in the copolymer would be beneficial in curbing the extent of the unwanted quick initial release. Additionally one could conclude that the solubility of the drug was higher in the methacrylate polymers compared to PS and that the methacrylate units would favor the efficiency of drug loading.

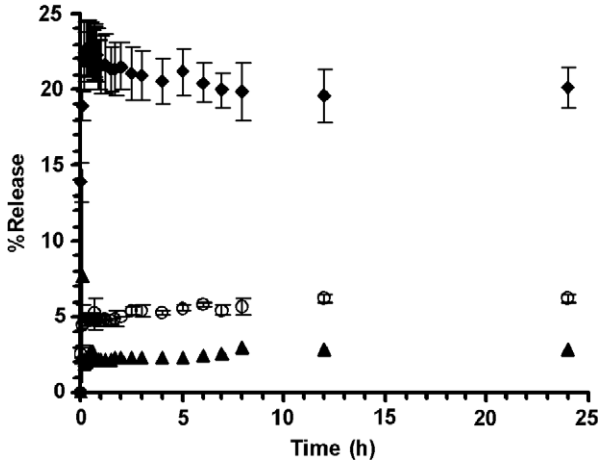

Fig. 9. Release profiles of RIF from ▲ PEMA, ○ PMMA and ♦ PS.

5.2. Copolymer films

5.2.1. Initial phase

The Peppas model was fitted to the release profiles and could not describe the initial release as a typical Fickian diffusion-controlled process during the initial release phase of the drug. These regressions produced exponent values of much lower than the expected exponents of $n = 0.5$. One could most probably state that a combination of diffusion and dissolution of surface molecules was possible for the drug that was not incorporated in the polymer film.

However, the $\Delta\delta$ value between the copolymer and the solvent/oligomer could reach a maximum value as the methacrylate content increased. This would result in a larger extrusion of solvent/oligomer during coacervation, finally depositing the drug on the surface. The higher prevalence of pores in P(St-*co*-EMA) could enhance this extrusion compared to P(St-*co*-MMA) up to certain critical composition. Furthermore, it was illustrated that polar solvent flux through copolymers of styrene and a more hydrophilic monomer could facilitate solvent pervaporation, therefore an increase in methacrylate levels could facilitate solvent and drug flux to surface of the film [59].

The initial release phases showed an approximate proportionality to an increase in the methacrylate content in both sets of the copolymers (Table 3). Additionally, no obvious relationship could be found to correlate the initial release phase with the contact angles of the copolymer films.

In contradiction to the homopolymer films, the copolymers resulted in drug release patterns that could be correlated to time at least for some part of the release profile. Fig. 10 displays the release patterns of RIF from P(St-*co*-EMA) and P(St-*co*-MMA) films, respectively. The most obvious observation was that both sets of polymer films released the drug in an initial phase at a high rate and then at a significantly slower rate for the remainder of the monitored period.

In both sets, two of the polymers released a high quantity of drug (~60% for EMA and ~70% for MMA copolymers)

Table 2
The release of drug in the initial and secondary release phases

	Initial (mg)[a]	$R_{initial}$ (%)[b]	Secondary (mg)[c]	%Load[d]	%wt/wt[e]
%EMA					
P(St-co-EMA) (onset of secondary phase at ~6 h)					
14	17.4	37.8	10.8	62.2	12.4
24	17.5	43.5	9.9	56.5	11.3
34	17.2	68.5	5.4	31.5	6.3
%MMA					
P(St-co-MMA) (onset of secondary phase at ~3 h)					
19	17.4	15.3	14.8	84.7	16.9
37	17.3	19.5	13.9	80.5	16.1
52	17.2	75.5	4.22	24.5	4.9

[a] The average amount of drug per film strip ($n = 3$).
[b] The average % release of the initial dose.
[c] Amount of drug capture in micropockets at onset of secondary release phase.
[d] Percent of drug available for controlled release.
[e] Concentration of drug in film at onset of controlled release.

Table 3
Kinetic parameters calculated for the secondary phase of RIF release from the various copolymer films

	Zero-order				Higuchi	
	r^2	k_0 (%/day)[a]	$t_{1/2}$ (days)	t_{max} (days)[b]	r^2	k (μg/cm^2/h$^{1/2}$)
%EMA						
P(St-co-EMA)						
14	0.9964	14.27 (0.49)	3.5	7.0	0.9901	34.42
24	0.9949	9.463 (0.38)	5.3	10.6	0.9919	31.06
34	0.9797	0.631 (0.06)	79	158.4	0.9562	1.290
%MMA						
P(St-co-MMA)						
19	0.9939	5.801 (1.21)	8.6	17.2	0.9916	8.748
37	0.9944	2.868 (0.10)	17.4	34.9	0.9906	3.966
52	obscured					

[a] All k_0 values in the table are statistically different from each other ($p < 0.05$).
[b] t_{max} is the calculated time required for complete release of the matrix-captured drug via zero-order kinetics.

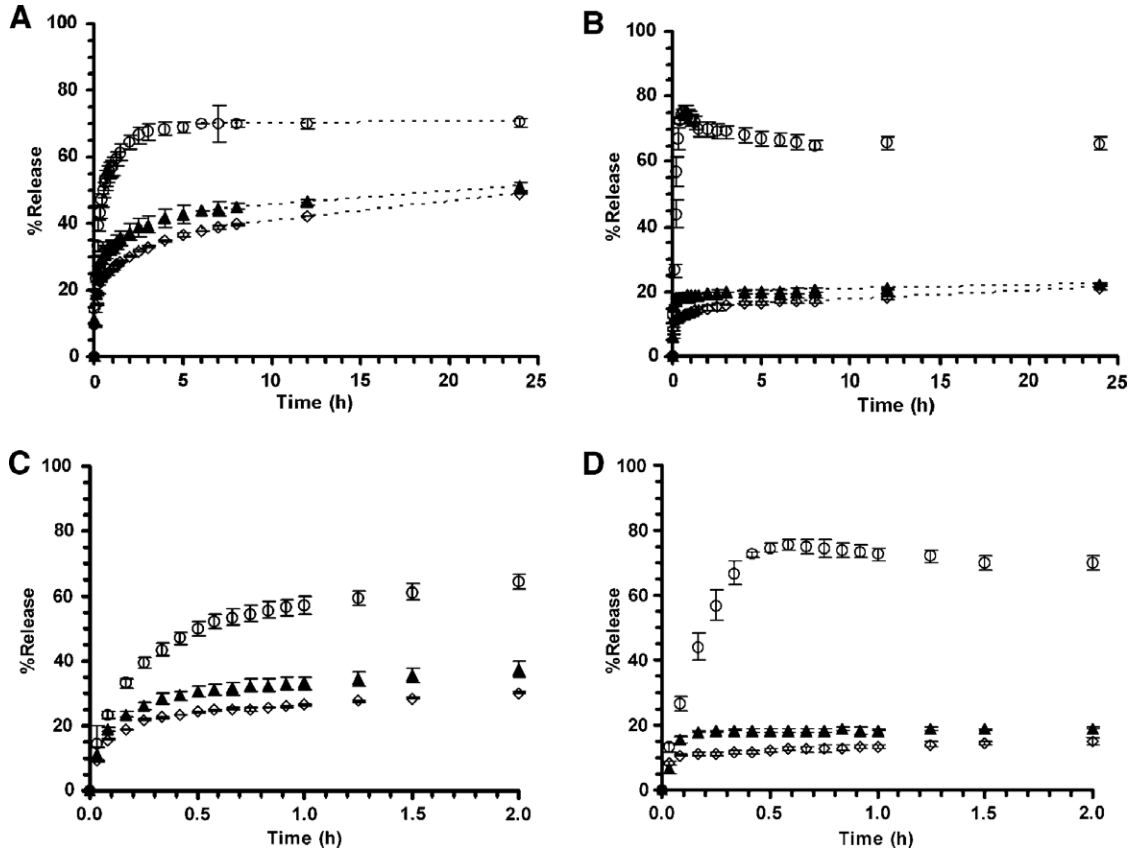

Fig. 10. (A–C) Release profiles (24 h) of RIF from films of (A) P(St-*co*-EMA) comprising of ○ 14%, ▲ 24% or ◇ 34% EMA (B) P(St-*co*-MMA) comprising of ◇ 19%, ▲ 37% or ○ 52% MMA and expanded views of the release profiles within the first 2 h of release (C) P(St-*co*-EMA) (○ 14%, ▲ 24% or ◇ 34% EMA) and (D) P(St-co-MMA)(◇ 19%, ▲ 37% or ○ 52% MMA).

within the first hour and this corresponded to the highest content of the methacrylate in the copolymer, i.e. 34% EMA and 52% MMA, respectively. It could be suggested that a large fraction of drug was deposited in the surface cavities of the 52% MMA film (Fig. 11A and B) and a large fraction of the drug in cavities on the film surface for the 34% EMA composition (Fig. 11C). This would indicate a limit in the methacrylate content if the release of drug should be controlled over an extended period (Table 2).

Indeed the amount of initial release was lower for the copolymers that contained the low and intermediate content of the methacrylates i.e. 14% EMA and 24% EMA for P(St-*co*-EMA), 19% MMA and 37% MMA for P(St-*co*-MMA).

The release profiles of the 14% and 24% EMA content P(St-*co*-EMA) films indicated approximately 40% release within the first 6 h or release before a zero-order rate of release was observed. On the contrary, approximately

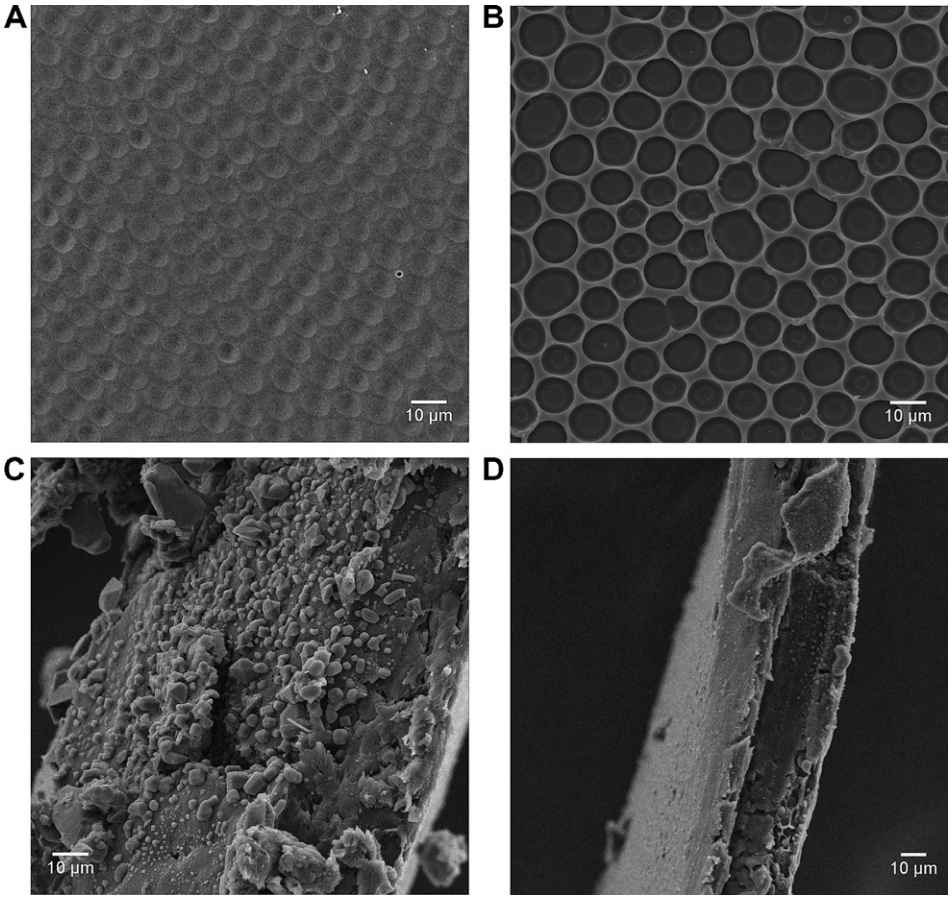

Fig. 11. Surface of RIF-loaded P(St-*co*-MMA) films (52% MMA) (A) before release and (B) after release. (C) Surface deposition of a RIF-loaded P(St-*co*-EMA) (34% film) before the release study was performed. (D) Film surface of RIF-loaded P(St-*co*-EMA) (34% film) after the release study was completed. The surface is smoother, with a few micropockets visible.

20% initial release was measured for the 19% and 37% MMA content P(St-*co*-MMA) films, before a stable release tempo could be obtained after 3 h. The morphology of the films could play some role in this release phase since the P(St-*co*-EMA) films illustrated a more porous material compared to the MMA copolymer films.

It was concluded that P(St-*co*-EMA) films should not exceed a composition of more than 24% EMA and P(St-*co*-MMA) should not incorporate more than 37% MMA in order to curb a high, unwanted initial release phase for films that were cast from an initial 20% drug/80% polymer mixture. The different sets of copolymers could however be employed to provide a different quantity of initial drug release, followed by prolonged release. The second phase of release will now be discussed to determine the usefulness of the copolymer films as sustained drug delivery systems.

5.2.2. Secondary phase

For the discussion here, the assumption was made that the initial phase considered the drug molecules that were released primarily without being controlled by the polymer film matrix. Therefore, the secondary phase considered the release of the drug molecules that was successfully loaded into the polymer film.

Despite the larger initial release of drug from the copolymers compared to the homopolymers, they could still provide the advantage of drug release during the second phase of release. More importantly, these copolymers show potential to control the release of drug at a predictable rate. Inspection of Fig. 10 revealed a strong tendency towards zero-order release for P(St-*co*-EMA) and P(St-*co*-MMA) films, respectively.

At the initial point of zero-order release one could find an approximate loading of the drug in the polymer matrix. At this point one could state that all the drug molecules that were not incorporated in the matrix have now been released and that the remaining drug molecules will now be released by the matrix according to the properties of the matrix. Table 3 lists the release values obtained for the secondary release phase of the various films.

The percentage of drug that was effectively captured in the matrix could be calculated and this is often described as the drug load. Table 2 reports the percentage of RIF that was successfully captured in the copolymer film micropockets. The percentage load of the drug corresponded closely to the copolymer composition with a decrease in the drug load as methacrylate concentration increased (or styrene content decreased). This illustrated one advantage for

the copolymer films over the homopolymer films in that the homopolymer could incorporate a larger quantity of drug in the matrix, however with no apparent extended release pattern.

Clearly, the zero-order release rate also decreased as the RIF captured in the film micropockets in the different copolymer films decreased suggesting a diffusion-type release pattern. Having performed a log-transformation of the concentration values in the second phase and fitting a log-linear curve to the data, an inferior fit was found compared to a zero-order (simple linear concentration). Since the concentration values of the drug was far below the solubility of the drug, it was concluded that the zero-order mechanism was valid This zero-order kinetic phase seemed plausible with consideration that the solubility of the drug at 1.5 mg/mL for the commonly found crystalline form II and the solubility of the amorphous form prepared from THF solutions 0.195 mg/ml [35,36] and with replacement of the sample volume with fresh buffer to maintain sink conditions. The maximum concentration that was achieved in this study was never higher than in the lower 30 μg/mL.

Subsequently the release data were converted to illustrate the flux of drug from a fixed surface of 30 cm^2 versus the square root of time. These Higuchi plots for P(St-*co*-EMA) and P(St-*co*-MMA) films (Fig. 12A and B) illustrated a good fit with $r^2 > 0.95$ for all curves. Higuchi kinetics describes the diffusion of molecules through a polymer matrix to the surface of the matrix with the diffusion distance increasing an infinitesimal amount per unit time towards the core of the matrix.

The thickness of the films measured was 40 ± 2 μm for all films and the films did not degrade in the release medium. Thus, the assumption was made that the film thickness remained constant and that the diffusion distance to the film surface did not vary significantly. The fact that zero-order release kinetics showed slightly better fits of the data ($r^2 > 0.97$), one could conclude that the diffusion of dissolved drug molecules to the release medium was regulated by the polymer barrier, therefore resulting in zero-order release.

Closer analysis of the second, controlled-release phase also revealed correspondence to copolymer composition. An inverse relationship was seen between the zero-order release rates and the concentration of the methacrylate in the P(St-*co*-EMA) films (Fig. 13). The conclusion was made that the methacrylate did indeed decelerate the zero-order release rate, a fact that was suggested by the drug release from PMMA and PEMA. Since the drug loads decreased as a function of methacrylate content in the copolymer, it is suggestive that diffusion rate was determined by the load, again indicating a diffusion-controlled release mechanism maintained by copolymer properties.

It could be predicted from the zero-order release rates that 35% EMA would be the maximum concentration in the copolymer if any zero-order phase release was expected for RIF. Additionally it would seem that the content of

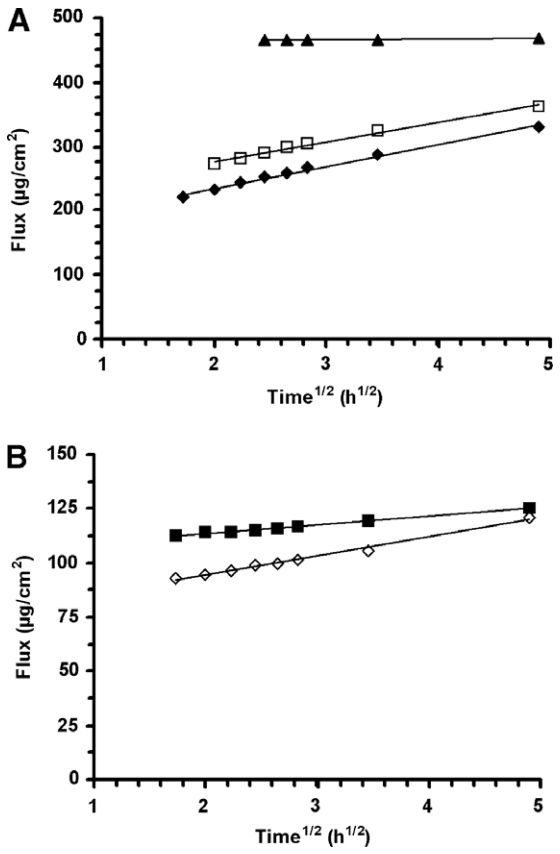

Fig. 12. Higuchi release plots of RIF after initial release from (A) P(St-*co*-EMA) comprising of ♦ 14%, □ 24% or ▲ 34% EMA and (B) P(St-*co*-MMA) comprising of ◇ 19 or ■ 37% MMA. Error bars are too small to display on this scale.

MMA in copolymers could be higher that that of the EMA in order to still obtain zero-order release.

The P(St-*co*-MMA) films illustrated lower release rates (~0.5-fold) compared to the P(St-*co*-EMA) films with higher quantities of drug captures in the P(St-*co*-MMA) films. These systems could probably be suited for longer-term use i.e. coating of prosthetic implants or medicated devices as seen from the calculated $t_{0.5}$ values

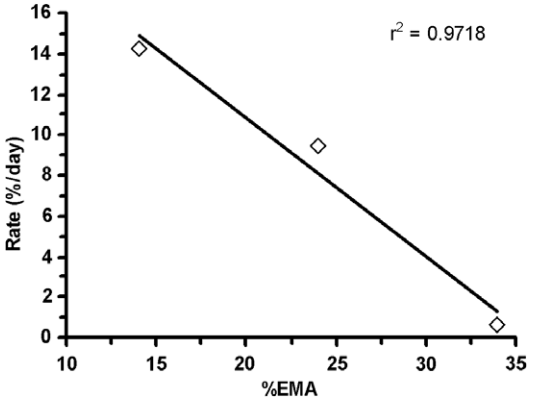

Fig. 13. The dependence of zero-order release on copolymer composition of P(St-*co*-EMA).

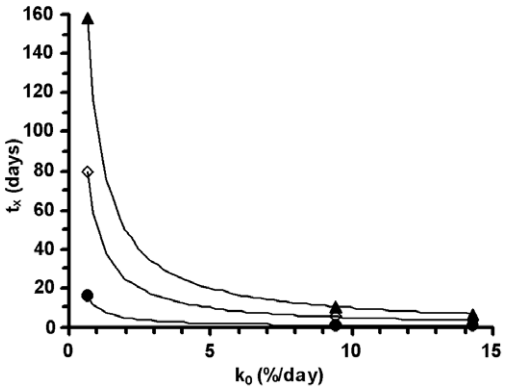

Fig. 14. Predicted release periods for RIF from P(St-*co*-EMA) for ● 10, ◇ 50 or ▲ 100% of RIF loaded in the film at the onset of zero-order release.

of 8.6 and 17.4 days for the 19% and 37% MMA films, respectively.

The P(St-*co*-EMA) films could release a higher quantity of drug over a shorter period of time. This could indicate shorter term applications such as application in temporary urinary catheters predicting a maximum usage period of 7–10 days for the 14% EMA and 24% EMA P(St-*co*-EMA) films, respectively. Fig. 14 shows the predicted release periods that were calculated from the zero-order rate constants for RIF from the P(St-*co*-EMA) films.

6. Conclusion

A series of nanosized styrene-methacrylate copolymers with molecular weights in the 10^2 kg mol^{-1} range were synthesized by microemulsion copolymerization. The cosurfactant dominated the size and weight properties of these copolymers due to induction of micellar coagulation during the reaction. Additionally, copolymer composition was primarily determined by the monomer feed ratio, however with some deviation from the feed. All these copolymers resulted in the formation of pseudolatexes if dissolved in THF as was indicated by the prevalence of the θ conformation of the copolymer chains as determined by GPC-MALLS.

The $\Delta\delta$ values, suggested that all components were miscible in THF. However, casting of the nanoscale drug-loaded pseudolatexes resulted in coacervation, phase separation of the drug and copolymer species and finally microenscapsulation of the drug. The solvent THF was thus crucial for the formation of a molecular dispersion of the components (as based on $\Delta\delta$), however, upon evaporation the surface free energy differences between RIF and copolymer resulted in phase separation of the drug and copolymer. Additionally, the copolymeric microcapsule walls interpenetrated resulting in a film that bridged yet another size hierarchy into the macroscale region.

No detrimental physical interaction between the drug and copolymers could be illustrated. The copolymer composition determined the magnitude of the initial release phase, subsequently also that of the second release phase. The second phase seemed to be a diffusion-controlled zero-order release phase. Predictions of release patterns showed that the copolymers could be useful in delivering drugs at zero-order release rate for a few days up to a few months.

As a compromise to their lower loading capacity, P(St-*co*-EMA) demonstrated a decrease in the contact angle upon incorporation of the drug or an increase in the EMA content. The use of these copolymers therefore seems promising despite their comparatively shorter controlled release phase. Different applications may be realized for these copolymers, i.e. short-term use as catheter coatings or long-term employment in implants.

References

[1] C.R. Arciola, Y.H. An, D. Campoccia, M.E. Donati, L. Montanaro, Etiology of implant orthopedic infections: a survey on 1027 clinical isolates, Int. J. Artif. Organs 28 (11) (2005) 1091–1100.
[2] G. Reid, H.J. Busscher, S. Sharma, M.W. Mittelman, S. McIntyre, Surface properties of catheters, stents and bacteria associated with urinary tract infections, Surf. Sci. Rep. 21 (1995) 251–273.
[3] D.S. Jones, J.G. McGovern, A.D. Woolfson, C.G. Adair, S.P. Gorman, Physicochemical characterization of hexetidine-impregnated endotracheal tube poly(vinyl chloride) and resistance to adherence of respiratory bacterial pathogens, Pharm. Res. 19 (6) (2002) 818–824.
[4] A. Jegatheeswaran, B. Jagdish, Pathology of infectious and inflammatory diseases in prosthetic heart valves, Cardiovasc. Pathol. 15 (5) (2006) 252–255.
[5] J.M. Schierholz, C. Morsczeck, N. Brenner, D.P. Konig, N. Yucel, M. Korenkov, E. Neugebauer, A.F.E. Rump, G. Waalenkamp, J. Beuth, G. Pulverer, S. Arens, Special aspects of implant-associated infection in orthopedic surgery. From the pathophysiology to custom-tailored prevention strategies, Der. Orthopade. 33 (4) (2004) 397–404.
[6] M. Henriques, N. Cerca, J. Azeredo, R. Oliveira, Influence of subinhibitory concentrations of antimicrobial agents on biofilm formation in indwelling medical devices, Int. J. Artif. Organs 28 (11) (2005) 1181–1185.
[7] C.R. Arciola, Why focus on implant infections? Int. J. Artif. Organs 28 (11) (2005) 1061.
[8] L.D. Christensen, C. Moser, P.Ø. Jensen, T.B. Rasmussen, L. Chirstophersen, S. Kjelleberg, N. Kumar, N. Høiby, M. Givskov, T. Bjarnsholt, Impact of *Pseudomonas aeruginosa* quorum sensing biofilm persistence in an in vivo intraperitoneal foreign-body infection model, Microbiology 153 (2007) 2312–2320.
[9] N.R. James, A. Jayakrishnan, Surface thiocyanation of plasticized poly(vinyl chloride) and its effect on bacterial adhesion, Biomaterials 24, 2205-2212.
[10] J.M. Schierholz, G. Pulverer, Investigation of a rifampin, fusidic-acid and mupirocin releasing silicone catheter, Biomaterials 19 (1998) 2065–2074.
[11] I. Raad, R. Darouiche, R. Hachem, M. Mansouri, G.P. Bodey, The broad-spectrum activity and efficacy of catheters coated with minocycline and rifampin, J. Inf. Dis. 173 (1996) 418–423.
[12] C.V. Ragel, M. Vallet-Regí, In vitro bioactivity of and gentamicin release from glass-polymer-antibiotic composites, J. Biomed. Mater. Res. 51 (2000) 424–429.
[13] L.C. Li, J. Deng, D. Stephens, Polyanhydride implant for antibiotic delivery – from the bench to the clinic, Adv. Drug. Deliv. Rev. 54 (2002) 963–986.
[14] D.M. Chilukuri, J.C. Shah, Local delivery of vancomycin for the prophylaxis of prosthetic device-related infections, Pharm. Res. 22 (4) (2005) 563–572.

[15] C.S. Kwok, T.A. Horbett, B.D. Ratner, Design of infection-resistant antibiotic-releasing polymers II. Controlled release of antibiotics through a plasma-deposited thin film barrier, J. Control. Release 62 (1999) 301–311.
[16] S. Bayoudh, A. Othmane, F. Bettaieb, A. Bakhrouf, H.B. Ouada, L. Ponsonnet, Quantification of the adhesion free energy between bacteria and hydrophobic and hydrophilic substrata, Mater. Sci. Eng. C 26 (2006) 300–305.
[17] G.M. Bruinsma, H.C. van der Mei, H.J. Busscher, Bacterial adhesion to surface hydrophilic and hydrophobic contact lenses, Biomaterials 22 (2001) 3217–3224.
[18] C.A. Nguyen, Y.N. Konan-Kouakou, E. Alléman, E. Doelker, D. Quintanar-Guerrero, H. Fessi, R. Gurny, Preparation of surfactant-free nanoparticles of methacrylic acid copolymers used for film coatings, AAPS PharmSciTech 7 (3) (2006), article 63.
[19] P. Couvreur, C. Dubernet, F. Puisieux, Controlled drug delivery with nanoparticles: current possibilities and future trends, Eur. J. Pharm. Biopharm. 41 (1995) 2–13.
[20] S.D. Hong, C.M. Burns, Compatibility of polystyrene and poly(-methyl methacrylate) in benzene. Effects of molecular weight and temperature, J. Appl. Polym. Sci. 15 (8) (1971) 1995–2006.
[21] K.L. Foster, R.P. Wool, Strength of polystyrene–poly(methyl methacrylate) interfaces, Macromolecules 24 (6) (1991) 1397–1403.
[22] W.C. Johnson, J. Wang, Z. Chen, Structures and properties of polystyrene/poly(methyl methacrylate) blends and copolymers, J. Phys. Chem. B 109 (2005) 6280–6286.
[23] R.L. Oréfice, A.P.C. Barbosa, M.M.N. Noguiera, Controlling the phase stability of polymer blends through the introduction of impenetrable surfaces, J. Appl. Polym. Sci. 187 (2003) 1619–1627.
[24] Y. Zhang, T. Guo, G. Hao, M. Song, B. Zhang, Nanosize polymer latexes made by microemulsion copolymerization: preparation and characterization, J. Appl. Polym. Sci. 90 (13) (2003) 3625–3630.
[25] M. Dittgen, M. Durrani, K. Lehmann, Acrylic polymers. A review of pharmaceutical applications, S.T.P. Pharma Sci. 7 (6) (1997) 403–437.
[26] M. Baleani, C. Persson, L. Guandalini, E. Piazza, P. Erani, S. Squarzoni, M. Viceconti, The effect of gentamicin sulphate on the fracture properties of manually mixed bone cement, Fatigue Fract. Eng. Mater. Struct. 30 (6) (2007) 479–488.
[27] K. Tauer, A.G. Ramírez, R.G. López, Effect of the surfactant concentration on the kinetics of oil in water microemulsion polymerization: a case study with butyl acrylate, C.R. Chim. 6 (2003) 1245–1266.
[28] P.J. Wyatt, Light scattering and the absolute characterization of macromolecules, Anal. Chim. Acta 272 (1) (1993) 1–40.
[29] A. Karami, S.T. Balke, T.C. Schunk, Quantitative interpretation of Fourier-transform infrared spectroscopic data from a size-exclusion chromatography solvent-evaporation interface, J. Chromatogr. A 911 (1) (2001) 27–37.
[30] Image J 1.38x. National Institutes of Health, USA. Available from: http://rsb.info.nih.gov/ij/.
[31] T. Wu, Y. Sun, N. Li, M.M. de Villiers, Y. Lian, Inhibiting surface crystallization of amorphous indomethacin by nanocoating, Langmuir 23 (2007) 5148–5153.
[32] G. Zografi, S.S. Tam, Wettability of pharmaceutical solids: estimates of solid surface polarity, J. Pharm. Sci. 65 (8) (1976) 1145–1149.
[33] The United States Pharmacopeia XXIX, The United State Pharmacopeial Convention, Inc. Rockville, MD, 2006.
[34] S.Q. Henwood, W. Liebenberg, L. Tiedt, A.P. Lötter, M.M. de Villiers, Characterization of the solubility and dissolution properties of several new rifampicin polymorphs, solvates, and hydrates, Drug Dev. Ind. Pharm. 27 (10) (2001) 1017–1030.
[35] S.Q. Henwood, M.M. de Villiers, W. Liebenberg, A.P. Lötter, Solubility and dissolution properties of generic rifampicin raw materials, Drug Dev. Ind. Pharm. 26 (4) (2001) 403–408.
[36] P.L. Ritger, N.A. Peppas, A simple equation for description of solute release. I. Fickian and non-Fickian release from non-swellable devices in the form of slabs, spheres, cylinders or disks, J. Control. Release 5 (1) (1987) 23–36.
[37] P.L. Ritger, N.A. Peppas, A simple equation for description of a solute release. II. Fickian and anomalous release from swellable devices, J. Control. Release 5 (1) (1987) 37–42.
[38] T. Higuchi, Rate of release of medicaments from ointment bases containing drugs in suspension, J. Pharm. Sci. 50 (1961) 874–875.
[39] T. Higuchi, Physical chemical analysis of percutaneous absorption process from creams and ointments, J. Soc. Cosmet. Chem. 11 (1960) 85.
[40] J.R. Robinson, S.P. Eriksen, Theoretical formulation of sustained-release dosage forms, J. Pharm. Sci. 55 (11) (1966) 1254–1263.
[41] G. Di Colo, Controlled drug release from implantable matrices based on hydrophobic polymers, Biomaterials 13 (12) (1992) 850–856.
[42] R. Marinov, S. Panayotova, A. Derzhanski, The phase behavior of the Triton X-114–water system and the hydrophile–llpophile balance theory, Prog. Colloid Polym. Sci. 118 (2001) 256–259.
[43] I.A. Mawell, B.R. Morrison, D.H. Napper, R.G. Gilbert, Entry of free radicals into latex particles in emulsion polymerization, Macromolecules 24 (1991) 1629–1640.
[44] C. Clasen, W.-M. Kulicke, Determination of viscoelastic and rheo-optical material functions of water-soluble cellulose derivatives, Prog. Polym. Sci. (2001) 1839–1919.
[45] Y. Liu, S. Bo, Y. Zhu, W. Zhang, Determination of molecular weight and molecular sizes of polymers by high temperature gel permeation chromatography with a static and dynamic laser light scattering detector, Polymer 44 (2003) 7209–7220.
[46] S. Grcev, P. Schoenmakers, P. Iedema, Determination of molecular weight and size distribution and branching characteristics of PVAc by means of size exclusion chromatography/multi-angle laser light scattering (SEC/MALLS), Polymer 45 (2004) 39–48.
[47] P.J. Flory, Principles of Polymer Chemistry, Cornell University Press; Ithica, NY, p. 672.
[48] X.J. Xu, F. Chen, Preparation of nanoparticles of poly(methyl methacrylate) latexes at θ condition, Langmuir 20 (2004) 528–531.
[49] N.S. Fernandes, M.A. da Silva Carvalho Filho, R.A. Mendes, M. Ionashiro, Thermal decomposition of some chemotherapeutic substances, J. Braz. Chem. Soc. 10 (1999) 459–462.
[50] L.S. Wigman, X. Zhang, D.O. Fisher, S.W. Walinsky, ICH guideline: harmonization of residual solvents in pharmaceuticals, Pharm. Technol. 20 (10) (1996) 102, 104, 106, 108.
[51] J.A. Gonzalez-Leon, A.M. Mayes, Phase behavior of ternary polymer mixtures, Macromolecules 36 (2003) 2508–2515.
[52] D.L. Ho, C.J. Glinka, New insights into Hansen's solubility parameters, J.. Polym. Sci. Part B: Polym. Phys. 42 (2004) 4337–4343.
[53] J.M. Schierholz, Physico-chemical properties of a rifampicin-releasing polydimethylsiloxane shunt, Biomaterials 18 (1997) 635–641.
[54] D.J. Greenhalgh, A.C. Williams, P. Timmins, P. York, Solubility parameters as predictors of miscibility in solid dispersions, J. Pharm. Sci. 88 (1999) 1182–1190.
[55] A.R. Shultz, P.J. Flory, Phase equilibria in polymer–solvent systems, J. Am. Chem. Soc. 74 (1952) 4760–4767.
[56] S.M. Safwat, S.S. Tous, I.A. Hassan, Preformulation of antituberculosis drugs in polymeric based blends, Bull. Pharm. Sci. Assiut Univ. 17 (1994) 127–138.
[57] B.B. Barik, B.K. Gupta, M. Pal, Preparation and in vitro dissolution of Eudragit RS micropellets containing rifampicin, S.T.P. Pharma Sci. 3 (1993) 472–476.
[58] H.O. Ammar, R.M. Khalil, Preparation and evaluation of sustained-release solid dispersions of drugs with Eudragit polymers, Drug Dev. Ind. Pharm. 23 (1997) 1043–1054.
[59] S. Ray, S.K. Ray, Effect of copolymer type and composition on separation characteristics of pervaporation membranes – a case study with separation of acetone–water systems, Journal of membrane science 270 (2006) 73–87.